Calibration Strategy and Efficiency Measurement of the Muon Identification Procedure at LHCb

A. Sarti, S. Furcas, G. Lanfranchi, M. Palutan

INFN - Laboratori Nazionali di Frascati, Italy

Abstract

We present a strategy for calibrating with data the LHCb muon identification procedure and for extracting in-situ the performance. Two main calibration samples are used: the inclusive $J/\psi \to \mu\mu$ decay as a source of muons and the $\Lambda(1115.6) \to p\pi^-$ decay as a source of hadrons decaying and non-decaying in flight. For each of them we describe the selection, the expected purity and the rates for different running scenarios. The distributions extracted from calibration samples are compared with those obtained from a generic b-inclusive sample. An estimate of the precision that can be reached in the evaluation of the muon identification efficiency and misidentification rate is given as a function of the collected statistics.

Contents

1 Introduction

Understanding the muon identification (muonID) efficiency with a percent precision at the earlier stages of the LHCb operations may be a challenging, if not impossible, task if one attempts to evaluate it by plugging into the detector simulation all the relevant details of detector performance and associated uncertainties.

Such simulation would have to include realistic modeling of geometry, detector edge effects, dead or noisy channels, non-optimal working point of some parts of the detector. Moreover all these effects are expected to change with time.

It is therefore mandatory to develop a procedure to measure with data the muonID efficiency and calibrate the relevant quantities necessary to ensure the best possible performance. This can be obtained by using reference processes with large production cross-section, like the inclusive $J/\psi \to \mu\mu$ and $\Lambda(1115.6) \to p\pi^-$ decays[1].

The muon identification procedure of the LHCb experiment is described elsewhere [1]. In the present note we describe a possible way to calibrate it and measure its performance with data using control samples.

The note is structured as follows: in Section 2 we briefly remind the reader of the main steps of the muon identification procedure. In Section 3 we describe the quantities that need to be calibrated and the calibration samples that will be used. In Section 4 we describe the Monte Carlo samples used for this study. In Section 5 we show the selection, the trigger, the expected purity and the rate as a function of the luminosity for the $J/\psi \to \mu\mu$ inclusive sample. In Section 6 we describe the selection procedure for the $\Lambda(1115.6) \to p\pi^-$ decay and show the rate and purity.

Two Sections (Section 5.5 and Section 6.4) show the expected precision in the measurement of the muonID efficiency and misidentification rate as a function of the collected statistics and address some possible sources of systematics.

In Section 7 and Section 8 we show the statistics needed to calibrate the main quantities and we compare the distributions extracted from calibration samples with the ones expected from Monte Carlo. Finally in Section 9 we draw the conclusions.

2 The muon identification procedure with first data

The muon identification procedure developed for the first data [1] consists of two main steps:

1. **IsMuonLoose selector:** hits in the muon stations are searched in some Field of Interest (FOI) around the track extrapolation. A boolean decision (*IsMuonLoose*) is applied to tracks which satisfy the requirement to have at least one hit in FOI in a number of stations which depends on the momentum of the track. The stations required by the *IsMuonLoose* decision are shown in Table 1 as a function of the

---

[1]The charge conjugate decay is always considered in the note.

track momentum. In Figure 1 we show the muonID efficiency curve as a function of the muon momentum after the IsMuonLoose selector.

momentum range	stations
3 GeV/c $< p <$ 6 GeV/c	at least one hit in FOI in at least two stations among M2,M3,M4
$p >$ 6 GeV/c	at least one hit in FOI in at least three stations among M2,M3,M4,M5

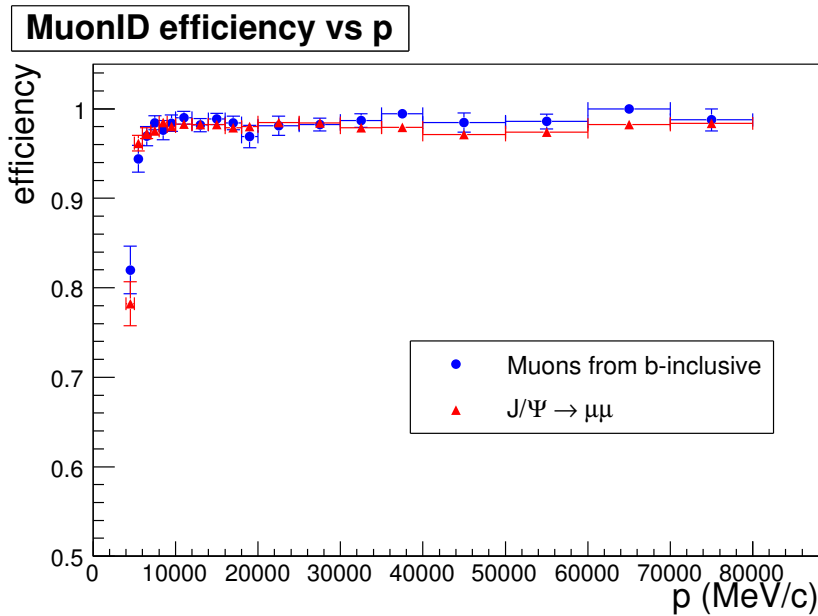Table 1: *IsMuonLoose* decision as a function of the momentum range.

Figure 1: MuonID efficiency curve versus p for b-inclusive (blue dots) and J/$\psi \to \mu\mu$ (red triangles) samples after the IsMuonLoose selector.

2. **The hypothesis test:** with tracks surviving the *IsMuonLoose* requirement, an hypothesis test is performed by evaluating for each track the compatibility with the muon and non-muon hypothesis [1].

   The hypothesis test is based on the average squared distance distributions of the hits in the muon chambers with respect to the extrapolation of the tracks from the tracking system. The average squared distance is defined as:

$$D = \frac{1}{N} \sum_{i=0}^{N-1} \left\{ \left(\frac{x_{closest,i} - x_{track}}{pad_x} \right)^2 + \left(\frac{y_{closest,i} - y_{track}}{pad_y} \right)^2 \right\} \qquad (1)$$

   where the i runs over the fired stations in the *IsMuonLoose* definition and $(x_{closest,i}, y_{closest,i})$ are the coordinates of the closest hit to the track extrapolation for each station.

The D distributions depend on the multiple scattering and, therefore, on the momentum and transverse momentum (or pseudo-rapidity) distributions of the analyzed sample: for this reason the hypothesis test is performed by binning the distributions in momentum bins and muon detector regions [1]. In Figure 2 we show an example of D distributions for the four muon detector regions and for two momentum bins.
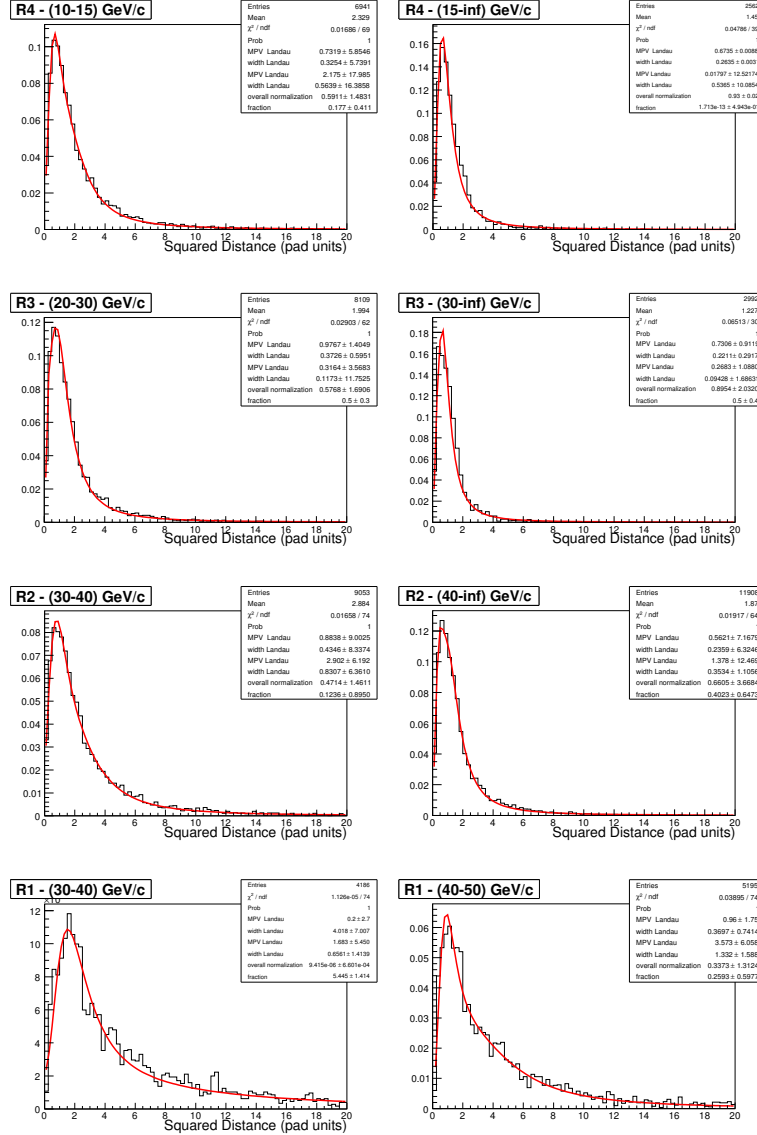

Figure 2: Average squared distance distributions for muons from a b-inclusive sample for the four muon detector regions and for two momentum bins.

3 The calibration of the muonID procedure

The monitoring of the performance of the muon identification procedure requires pure samples of muons and pure samples of hadrons, decaying and non-decaying in flight before the muon system. These samples have to cover all the interesting momentum range, have to illuminate the whole muon detector area and must be selected without using the muon system.

We plan to use the inclusive $J/\psi \to \mu\mu$ decay mode as a source of muons and the $\Lambda(1115.6) \to p\pi^-$ process as a source of hadrons decaying and non-decaying in flight. Both processes have large cross sections ($\sigma(pp \to J/\psi) \sim 290\mu b$, $\sigma(pp \to \Lambda X) \sim 10mb$) and therefore can be used also at the beginning of data taking when the luminosity will be low ($L < 10^{31}$ cm^{-2} s^{-1}). As soon as the luminosity reaches its nominal value we plan to use also the $D^{*+} \to D^0(K\pi)\pi^+$ process to evaluate the rate of fake muons coming from kaon misidentified. The selection of the $D^{*,+}$ decays is described in [2].

The selection of $J/\psi \to \mu\mu$ and $\Lambda(1115.6) \to p\pi^-$ calibration samples must not rely on any other particle identification procedure as it might not be calibrated when these samples are selected. So the selections described in the present note rely only on very basic quantities as tracks and energy released in the calorimeters.

The muon identification procedure needs to be calibrated periodically and continuously monitored during data taking. What we need to calibrate and how often is described in the following.

- **The Fields of Interests (FOI):** two curves (x and y views), 3 parameters each, as a function of the momentum for each muon detector region and station. In total we have to calibrate 40 curves, 3 parameters each [3].

  These curves depend on the tracking parameters which define the track extrapolation into the muon system and on the multiple scattering, which depends on the momentum and the material crossed by the track.

  In LHCb the whole tracking procedure will be re-aligned at every fill (every $\sim$8 hours) as the VELO is opened at the beginning of the fill and closed when the beam is declared stable in the orbit. Therefore the tracking parameters are expected to change at every fill. The accuracy in the determination of the tracking parameters in the point of closest approach to M1 in principle can affect the MuonID performance. However a detailed study of this effect will be possible only with data: for this reason the FOI will be continuously monitored and their parameters will be re-calibrated if the results are not stable.

  The FOI parameters are chosen as a compromise between the highest possible muon identification efficiency and a reasonable misidentification rate. Therefore if the background conditions affecting the misidentification rate change with time, the FOI size should change accordingly. The FOI have to be continuously monitored and their parameters have to be re-calibrated if the results are not stable.

- **The distance distributions used in the hypothesis test**.
  For these distributions the same considerations are valid as for the FOI. They depend on the tracking parameters, the multiple scattering and, for the non-muon sample, on the amount and spatial distribution of background hits in the muon chambers. In principle they should be monitored and calibrated every time the tracking parameters or background contamination change.

4   Monte Carlo samples

The Monte Carlo samples used in the present study are listed in Table 2.

channels	number of events	Configuration
J/$\psi \to \mu\mu$ inclusive	~ 140k	DC06-phys-v2-lumi2
Minimum Bias (MB)	$\sim 5.4 \times 10^6$	DC06-L0-v1-lumi2
bb-inclusive	~ 800k	DC06-L0-v1-lumi2

Table 2: Monte Carlo samples. The configuration refers to the LHCb bookkeeping database.

All the samples belong to the same Monte Carlo production set and have been produced assuming the nominal average luminosity of $L = 2 \times 10^{32}$ cm^{-2} s^{-1}. The tracks in all the samples have been preselected by requiring to be long or downstream tracks[2] with a minimum momentum of $p = 3$ GeV/c and pointing inside the muon detector acceptance.

5   The J/$\psi \to \mu\mu$ calibration sample

The J/$\psi \to \mu\mu$ inclusive decay is a process with a very clean signature and therefore it can be used as a pure source of muons. We use J/$\psi \to \mu\mu$ events with one muon identified by the muon system (*tag*) and the second muon selected without using the muon system (*probe*). The *probe* muon can be used for calibrating the muon identification procedure.

A similar *tag-and-probe* method is used in the ATLAS and CMS Collaborations which use high p_T muons from the $Y(4S) \to \mu^+\mu^-$ and $Z^0 \to \mu^+\mu^-$ processes for measuring the efficiency of the muon reconstruction from data [5, 6].

The inclusive J/ψ cross section expected at the LHC nominal energy [7] is $\sigma_{\mathrm{J/\psi}} \sim 286$ μb, where ~ 266 μb comes from the prompt J/ψ production and ~ 20 μb from the b-mesons decay $b \to$ J/ψ X. Given the $BR(\mathrm{J/\psi} \to \mu\mu) = (5.93 \pm 0.0.6)\%$ [8], and the probability that both muons are within the LHCb acceptance, $p_{\mathrm{acc}} \sim 10\%$, we have an effective cross-section of $\sigma_{\mathrm{J/\psi} \to \mu\mu} \sim 1.7$ μb which corresponds to a yield of $N_{\mathrm{J/\psi} \to \mu\mu} \sim 1.7 \times 10^6$ per pb^{-1} for events with both muons reconstructed, before considering trigger and selection.

---

[2]A track is *long* if it comes from the primary vertex and releases hits in all the tracking detectors, it is *downstream* if releases hits only in the TT and IT/OT detectors [4].

5.1 The trigger

In the J/$\psi \rightarrow \mu\mu$ sample the *probe* muon has to be selected without using the muon system. Therefore these events have to be triggered either by the other (*tag*) muon or by any other particle in the event not belonging to the J/$\psi \rightarrow \mu\mu$ decay.

A detailed discussion concerning the LHCb trigger is beyond the scope of this note but it is useful to review briefly here the general LHCb trigger structure and to discuss the trigger lines required for the J/$\psi \rightarrow \mu\mu$ selection.

The LHCb trigger is divided in two levels: Level-0 (L0) and High Level Trigger (HLT). The L0 selects events with high p_{T} muons or calorimeter objects (hadrons, pions, γ and electrons). At the nominal luminosity of 2×10^{32} cm^{-2} s^{-1} it reduces the input 40 MHz rate to 1 MHz. The HLT reduces the L0 output rate to 2 kHz.

5.1.1 The Level-0 trigger

With the present tuning at nominal running conditions ($L \sim 2 \times 10^{32}$ cm^{-2} s^{-1}) the L0-trigger accepts events which satisfy any of the following conditions:

- a muon candidate with a $p_{\mathrm{T}} > 1.5$ GeV/c (L0 single-μ);

- two muon candidates with $|p_{\mathrm{T},1}| + |p_{\mathrm{T},2}| > 1.5$ GeV/c (L0-diμ);

- a hadron detected in the hadronic calorimeter (HCAL) with $E_{\mathrm{T}} > 3.5$ GeV (L0-hadron);

- an electron or a photon detected in the electromagnetic calorimeter (ECAL) with $E_{\mathrm{T}} > 3.5$ GeV(L0-$\gamma, e^{\pm}$).

5.1.2 The HLT trigger

The HLT is divided in two levels, HLT1 and HLT2. The HLT1 is composed of several trigger paths, named "alleys", which are invoked depending on the nature of the object that fired the L0-trigger: muon, hadron, electron γ and π^0. Here we consider only the alley which selects muons. The purpose of the HLT1 muon alley is to confirm a L0-μ candidates using the tracking system. For confirmed events, the HLT1 muon alley accepts events satisfying any of the following conditions:

- **the single-μ line:** the confirmed L0-μ candidate has either an impact parameter IP>0.08 mm and a p_{T} >1.3 GeV/c or a very high p_{T} >6 GeV/c. In the low luminosity regime ($L \sim 10^{30} - 10^{31}$ cm^{-2} s^{-1}) the confirmed L0-μ candidate is required only to have a $p_{\mathrm{T}} > 1$ GeV/c.

- **the μ+track line:** the confirmed L0-μ candidate forms with another track a common vertex and an invariant mass $M_{\mu\mu} > 0.8$ GeV/c^2 in the di-μ mass hypothesis. Both the muon and the track are required to have an impact parameter and a p_{T} above certain thresholds: $p_T(\mu, \text{track}) > (1, 0.8)$ GeV/c and IP(μ, track)>(25,50)μm.

- **the di-μ line:** two candidate muons are found either with a distance of closest approach DOCA< 0.5mm and with an invariant mass $M_{\mu\mu}$ >2.5 GeV/c^2 or with an impact parameter IP>0.15 mm and with $M_{\mu\mu} > 0.5$ GeV/c^2.

The muon trigger lines suitable for the J/$\psi \to \mu\mu$ selection are those containing only one muon identified, e.g. the single-μ line or the μ+track line. The use of the single-μ line or the μ+track line depends on the luminosity conditions:

1. in the low luminosity regime ($L \sim [10^{30} - 10^{31}]$ cm^{-2} s^{-1}) we will use the single-μ trigger line which cuts only on the transverse momentum (p_T) of the candidate muon. In these conditions the signal is dominated by the prompt component of the J/$\psi \to \mu\mu$ process and the background is dominated by the prompt Minimum Bias (MB) background.

2. In the medium-high luminosity regime ($L \sim [10^{31} - 10^{32}]$ cm^{-2} s^{-1}) we will use the μ+track trigger line which requires also impact parameter cuts on the μ+track pair. In these conditions the trigger will select only J/$\psi \to \mu\mu$ events with displaced vertexes, i.e. from b-meson decays. The main background in this case is the long-lived component coming from b-mesons decays.

In the present note we consider both cases: the selection of the inclusive J/$\psi \to \mu\mu$ and the corresponding output rate are described in Section 5.2 and Section 5.3. The selection of J/$\psi \to \mu\mu$ from b-decays largely overlaps with the inclusive case but for the trigger selections and some offline cuts optimized to reject the combinatorial background from b-decays. This selection is described in Section 5.4.

5.2 The selection of the J/$\psi \to \mu\mu$ inclusive sample

In this Section we discuss the selection of the J/$\psi \to \mu\mu$ inclusive decay from a sample of minimum bias events.

The J/$\psi \to \mu\mu$ inclusive decay is selected in several steps: first a loose preselection is applied by requiring two good quality long tracks of opposite charge with $p > 3$ GeV/c, pointing inside the muon detector acceptance, originating from a common vertex and with an invariant mass ± 300 MeV/c^2 around the J/ψ nominal mass in the hypothesis of the muon mass (Table 3). At this stage no peak shows up in the invariant mass distribution, as it is shown in Figure 4 (solid line).

Then we exploit the fact that the muons from the J/ψ decay have on average higher p_T values than tracks from minimum bias (Figure 3, bottom-left): we require both muons have a $p_{T min} > 800$ MeV/c.

The L0-single muon trigger behavior is emulated by requiring that one of the two tracks crosses all the 5 muon stations (i.e. it has $p > 6$ GeV/c), is identified as a muon by the muon system[3] and has a $p_T > 1.5$ GeV/c. The L0-muon candidate is the *tag* muon.

---

[3]The condition *IsMuon =1* must be satisfied as described in [1].

2 long tracks with opposite charge
$\chi^2_{\text{trk}}/\text{nDoF} < 3$
$p_{\mu 1}$ and $p_{\mu 2} > 3$ GeV/c
$\chi^2/nDoF(J/\Psi) < 20$
$\vert M_{\mu\mu} - M_{J/\Psi}\vert < \pm 300$ MeV/c

Table 3: $J/\psi \rightarrow \mu\mu$ preselection cuts.

A substantial improvement is observed in the background rejection after the L0-emulation. This is shown in Figure 4 (green-dashed curve). In case of both tracks satisfying the L0 trigger, the one with the highest transverse momentum is chosen as a tag muon. When running the filter in the framework of the online software environment, the tag muon will be identified directly using the information provided by the trigger. Identification of the *tag* muon automatically defines the opposite charged track as the *probe* muon.

The energies deposited in the electromagnetic (ECAL) and hadronic (HCAL) calorimeters [9] are used as additional handles to select muons without using the muon system: in fact, since muons are Minimum Ionizing Particles (MIPs), this energy is a fixed quantity which depends only on the dE/dX in the calorimeter material.

In Figure 5 we show the energy deposited in ECAL and HCAL by muons coming from J/ψ (solid histograms), by all the tracks belonging to the MB background (solid line) and by the tracks belonging to the MB background but removing the contribution from decays in flight and from true muons not from J/ψ decay (dashed line). We see that in ECAL a MIP releases on average around ~ 400 MeV while in HCAL ~ 2200 MeV. The peaks at zero visible mainly in the ECAL distributions are due to the fact that below a certain polar angle the MIP signal goes below the calorimeter zero suppression thresholds and is not detected [10].

We require that the *probe* muon candidate releases in ECAL and HCAL an energy compatible with a MIP: $0 \leq E_{ECAL,\mu_{\text{probe}}} < 1\,\text{GeV}$ and $1\,\text{GeV} < \text{E}_{\text{HCAL},\mu_{\text{probe}}} < 4\,\text{GeV}$. This cut produces a clear improvement in the background rejection, shown in Figure 4 (dotted line).

The requests on the calorimeter energy are not applied to the tag muon candidate, since this track is already a muon in most of the cases. Moreover, this will give us the possibility to use the same sample for monitoring the MIP peaks and tuning the calorimeter selection cuts during data taking.

Further reduction of background, is obtained by requiring the probe muon track to have at least one hit in 2×FOI in M2 station (Figure 4, solid histogram). The signal is almost unaffected by this requirement. Negligible bias from this request on the value of muonID efficiency has been found on a sample of true muons from J/ψ. All of the previous cuts are listed in Table 4, with the corresponding efficiencies for $J/\psi \rightarrow \mu\mu$ and
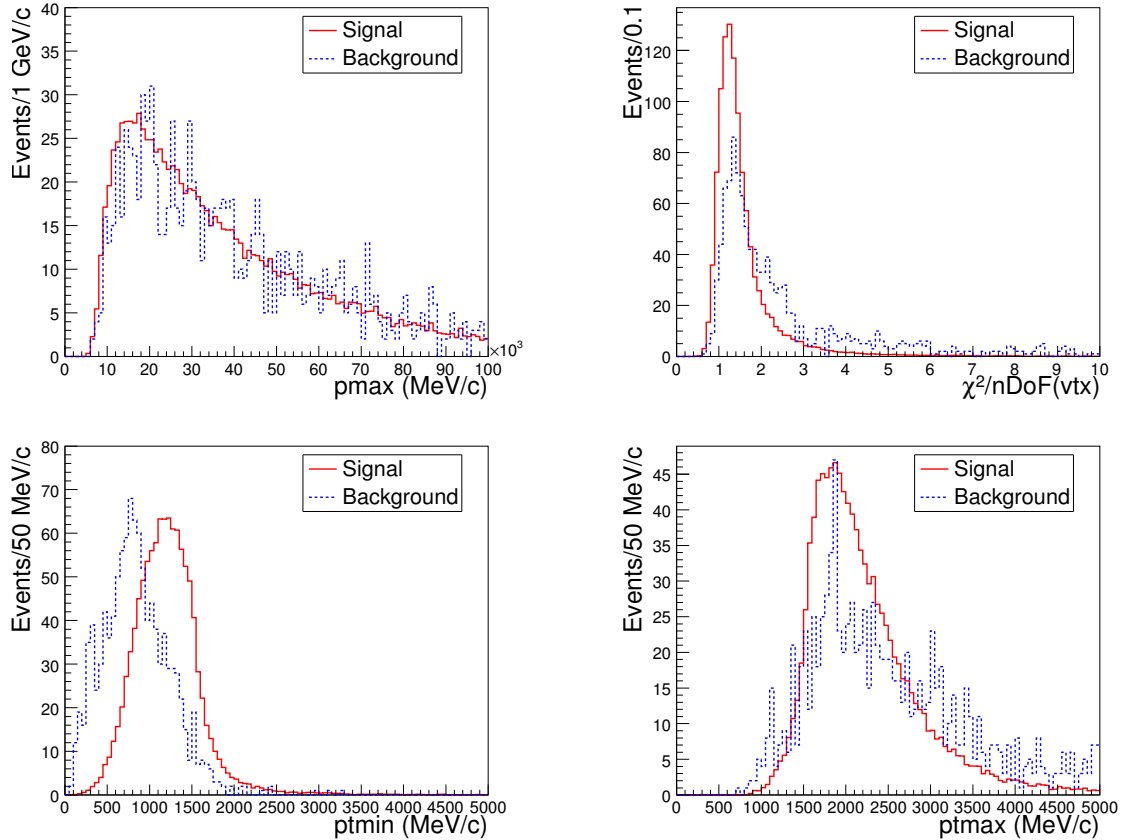
Figure 3: Distributions for signal ($J/\psi \to \mu\mu$) and background (Minimum Bias) of the maximum momentum of the muons pair (top-left), the χ^2/nDoF of the J/ψ vertex (top-right), the minimum (bottom-left) and the maximum transverse momentum (bottom-right) of the muons pair.

MB events. Each efficiency is normalized to the previous cut, the efficiency of the first cut is normalized to the preselected sample.

The invariant mass distribution of the selected events is shown in Figure 6. The number of signal (S) and background (B) events is extracted from a fit with a Gaussian shape for the signal plus an exponential which describes the background, with weights k_1 and k_2 respectively. The fitted parameters are shown in the Figure. The resolution on the J/ψ mass is $\sigma \sim 12$ MeV/c^2. From a sample of 5.4×10^6 L0-stripped MB events, we count 630 $J/\psi \to \mu\mu$ events in a $\pm 2\sigma$ mass window, with S/B ratio ~ 3.5. Restricting to a $\pm 1\sigma$ window, signal yield becomes 450, with a better S/B ratio, ~ 5.

The study of the composition of the background for the probe muon candidate using the Monte Carlo truth information shows that $\sim 42\%$ of background candidates are muons (either from π's and K's decays in flight or from b's and c's mesons semi-leptonic decays) and $\sim 58\%$ are non-muons. This composition is the same under the peak and in the
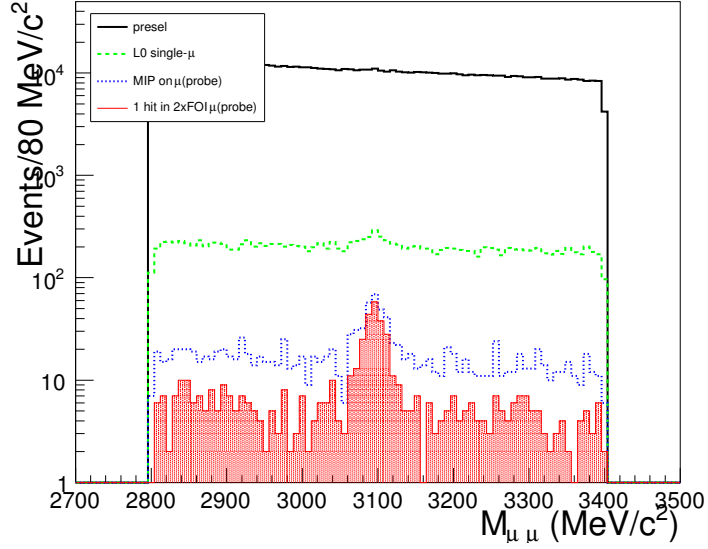
9

Figure 4: Di-μ invariant mass distribution as a function of the cuts applied during the selection (see text).

cut	$\epsilon(\mathrm{J}/\psi \to \mu\mu)$ [%]	ϵ(MB) [%]
$p_T(\mu_{1,2}) > 800$ MeV/c	87.1 ± 1.6	48.26 ± 0.03
L0-single μ (tag μ definition): $p_{T,\mu_{tag}} > 1.5$ GeV/c $p_{\mu_{tag}} > 6$ GeV/c IsMuon(μ_{tag}) = 1	91.6 ± 1.4	1.75 ± 0.01
calorimeter cuts, probe μ only: $0 \le E_{ECAL,\mu_{probe}} < 1000$ MeV 1000 MeV $< \mathrm{E}_{\mathrm{HCAL},\mu_{\mathrm{probe}}} < 4000$ MeV	74.7 ± 2.3	7.17 ± 0.16
1 hit in 2xFOI, probe μ	~ 100	60.9 ± 1.2
$\epsilon_{\mathrm{sel}} = N_{\mathrm{sel}}/N_{\mathrm{presel}}$	59.6 ± 2.3	0.037 ± 0.001

Table 4: Selection cut efficiencies normalized to the preselection (described in the text), for J/$\psi \to \mu\mu$ decays, and for MB events.

mass sidebands, so the sidebands can be used to evaluate the muonID performance on the background under the peak.

The momentum spectrum and the illumination of M2 station of the *probe* muon from ~ 140k J/$\psi \to \mu\mu$ events are shown in Figures 7-8. In Table 5 we show in which fraction the probe muon crosses a given detector region.
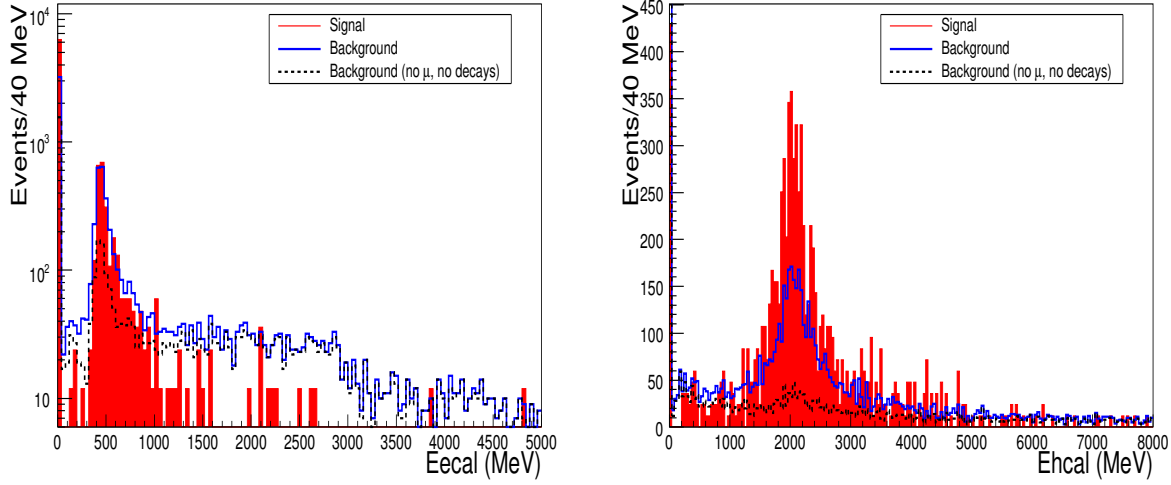
Figure 5: Energy deposited in the Electromagnetic Calorimeter (left) and in the Hadronic calorimeter (right) by muons from J/ψ (filled histograms), tracks from MB background (solid line) and tracks from MB background after the removal of decays in flight and muons not belonging to the J/$\psi \to \mu\mu$ decay (dashed line).

Region 1	6.2 ± 0.1 %
Region 2	$28.2 \pm 0.1\%$
Region 3	$36.0 \pm 0.1\%$
Region 4	$30.1 \pm 0.1\%$

Table 5: Fraction of *probe* muons crossing a given muon detector region.
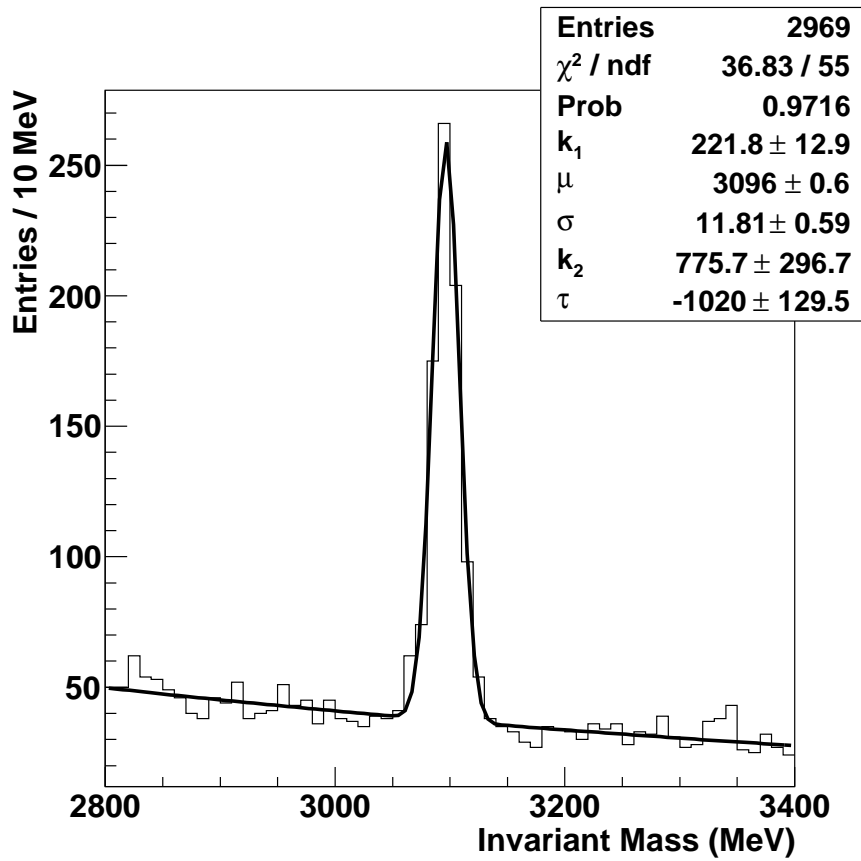
Figure 6: Invariant mass of the J/$\psi \to \mu\mu$ candidates selected from 5.4 millions of MB events after L0 trigger. Results of a fit to a Gaussian shape for the signal and exponential shape for the background, with weights k_1 and k_2 respectively, are superimposed.
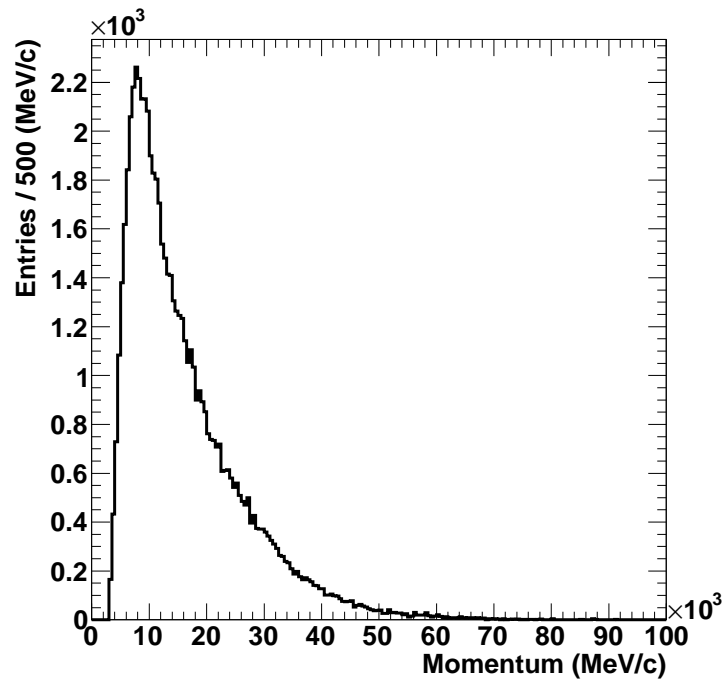
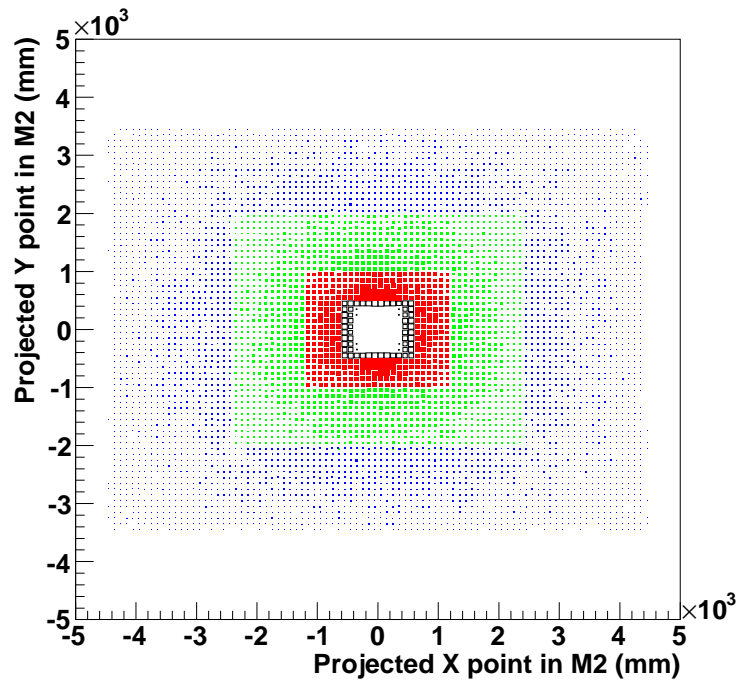Figure 7: Momentum spectrum of the probe muon after the selection.

Figure 8: Muon detector illumination of the probe muon after the selection.

13

5.3 The rate of the J/$\psi \to \mu\mu$ inclusive

The rate corresponding to the events selected by the cuts described in Table 4 in ± 300 MeV/c^2 mass window around the J/ψ mass can be calculated as follows:

$$R_{J/\psi} = \frac{N_{MB}(sel)}{(N_{MB}(input)/\epsilon_{MB}(L0))} \times R_{BC} \qquad (2)$$

where $N_{MB}(sel)$ are the number of events selected in ± 300 MeV/c^2 mass window, $N_{MB}(input) \simeq 5.4 \times 10^6$ are the initial number of MB events after $L0$ trigger, $\epsilon_{MB}(L0) = 5.9\%$ is the $L0$ efficiency on a MB sample, and R_{BC} is the rate of pp interactions.

At the nominal luminosity of $L = 2 \times 10^{32}$ cm^{-2} s^{-1} the rate of pp interactions at LHCb is $R_{BC} \sim 14.8$ MHz. In fact, the probability to have a bunch crossing with N_{pp} interactions is given by the Poisson distribution $P(\mu, N_{pp})$ where μ is the average number of interactions per crossing. The average number of interactions per crossing is given by $\mu = \sigma_{tot} \times L/r_{BC} - 0.694$, where $\sigma_{tot} = 102.9$ mb is the total pp interaction cross section, $L = 2 \times 10^{32}$ cm^{-2} s^{-1} is the average luminosity and the $r_{BC} = (2622./3564.) \times 40.08$ MHz ~ 29.5 MHz is the non-empty bunch crossing rate at LHCb. Therefore the rate of pp interactions is given by $R_{BC} = r_{BC} \times (1. - \mathrm{Poisson}(\mu, 0.)) \sim 14.8$ MHz.

This rate clearly depends on the run conditions, which in the 2009-2010 run will be very different from the nominal ones. In the upper part of Table 6 we show the average luminosity, the non-empty bunch crossings at the LHCb interaction point and the rate of minimum bias crossings R_{BC} corresponding to the expected running conditions in the 2009-2010 run (first three columns). In the fourth column we show the same quantities corresponding to nominal running conditions.

In the bottom part of Table 6 we show the expected rates of J/$\psi \to \mu\mu$ selected events calculated in the four scenarios with the Equation 2. In all scenarios we assume a nominal $\sqrt{s} = 14$ TeV center-of-mass energy and a L0 trigger working with nominal settings[4].

The events shown in Figure 6 can be collected in 10 minutes, 3 minutes, 40 seconds and 6 seconds of running in the low, medium, high and nominal luminosity conditions.

5.4 The selection of the J/$\psi \to \mu\mu$ from b−decays

As mentioned in the Section 5.1, in the medium-high luminosity regime ($L \sim [10^{31} - 10^{32}]$ cm^{-2} s^{-1}) the single-μ trigger line with only p_T cuts can be used only with a very high threshold for the p_T, typically $p_T > 6$ GeV/c, in order to control the rate.

In these conditions, it is more convenient to select J/$\psi \to \mu\mu$ events by using the μ+track trigger line. This line requires also impact parameters (IP) cuts on the μ+track pair and therefore selects mainly J/$\psi \to \mu\mu$ events with a displaced vertex, i.e. from b-mesons decays.

---

[4]We assume a L0 efficiency on minimum bias events of $\epsilon_{L0} = 5.9\%$.

	Low	Medium	High	nominal
L ($\times 10^{31}$ cm^{-2} s^{-1})	0.228	0.814	2.802	20
Bunches @ LHCb	19	68	468	2622
R_{BC} [kHz]	135.1	483.4	2070.8	14760
total (signal) rate in ±300 MeV/c^2	$\sim$5 (1.2) Hz	$\sim$16 (4) Hz	$\sim$70 (16) Hz	$\sim$500 (120) Hz

Table 6: Top: average luminosity, number of non-empty bunches colliding at the LHCb interaction point and rates of minimum bias crossings corresponding to the running conditions expected in the 2009-2010 run (first three columns) and to the nominal running conditions (fourth column). Bottom: total (signal) rate of J/$\psi \to \mu\mu$ candidates after the selection in ±300 MeV/c^2 mass window.

The selection of J/$\psi \to \mu\mu$ decays with displaced vertex follows exactly the same steps as for the inclusive selection (Table 4) with two differences:

1. we require the *tag* muon has a IP$> 80\mu$m and the *probe* muon an IP$> 50\mu$m;

2. a better quality for the J/ψ decay vertex, $\chi^2/nDoF(J/\Psi) < 6$ is required to suppress combinatorial background originating from b decays.

The invariant mass of J/$\psi \to \mu\mu$ candidates is shown in Figure 9. Results of a fit with a Gaussian shape for the signal, with weight k_1, plus a linear shape for the background, with intercept k_2 and slope τ, are superimposed. The S/B ratio in a $\pm2\sigma$ mass window is ~ 7.

The total event yield in a ±300 MeV/c^2 mass window corresponds to a rate of ~ 36 Hz at nominal luminosity, with ~ 13 Hz coming from J/$\psi \to \mu\mu$, $\sim 60\%$ of which from b. In the high luminosity scenario foreseen for the 2009-2010 run, $L \sim 2.8 \times 10^{31}$ cm^{-2} s^{-1}, the total output rate is ~ 5 Hz.

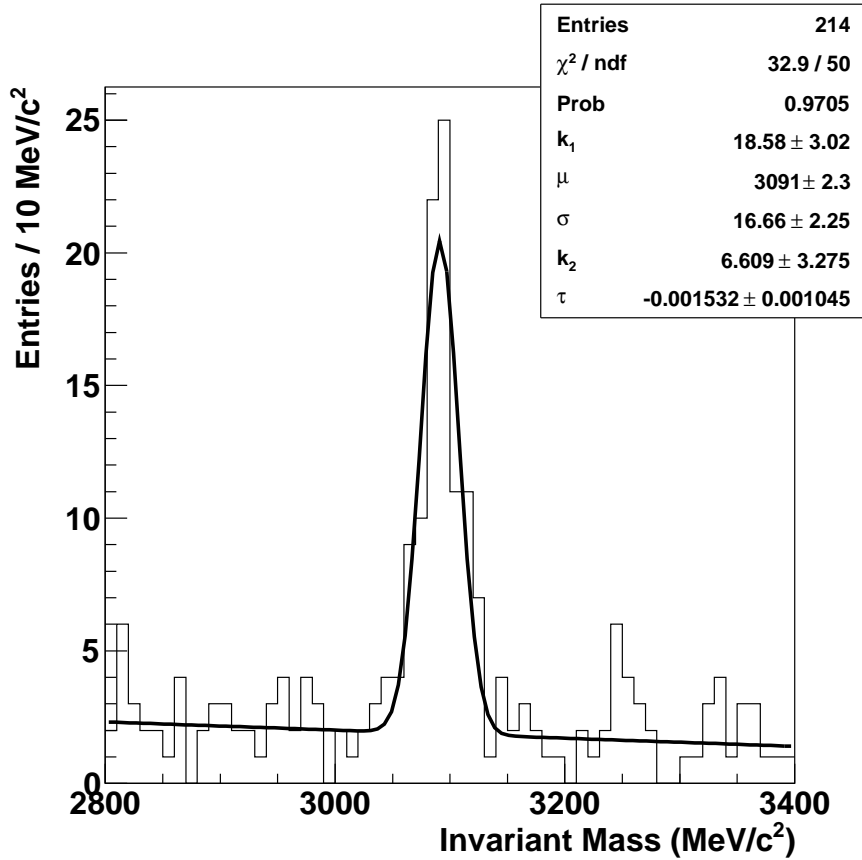| Entries	214
χ^2 / ndf	32.9 / 50
Prob	0.9705
k_1	18.58 ± 3.02
μ	3091 ± 2.3
σ	16.66 ± 2.25
k_2	6.609 ± 3.275
τ	-0.001532 ± 0.001045

Figure 9: Invariant mass of the J/$\psi \to \mu\mu$ candidates with detached vertex selected from 5.4 millions of MB events after simulation of L0 trigger and HLT1 μ+track line. Results of a fit with a Gaussian shape for the signal, with weight k_1, plus a linear shape for the background, with intercept k_2 and slope τ, are superimposed.

5.5 The measurement of the muonID efficiency

The muonID efficiency evaluation is performed by selecting $J/\psi \to \mu\mu$ candidates with a mass within a window of $\pm 1\sigma$ around the nominal J/ψ mass (where $S/B \sim 5$) and by requiring the *probe* muon candidates to pass the *IsMuonLoose* condition (Section 2). We find an efficiency $\epsilon_{S+B} = (86.0 \pm 1.5)\%$. When we require that the *probe* muon belongs to the $J/\psi \to \mu\mu$ decay we find $\epsilon_S^{true} = (97.4 \pm 0.8)\%$.

The difference between ϵ_{S+B} and ϵ_S^{true} is due to the background contamination. In fact the efficiency measured in a given mass window (ϵ_{S+B}) is related to ϵ_S by the following equation:

$$\epsilon_{S+B} = \frac{S}{S+B}\epsilon_S + \frac{B}{S+B}\epsilon_B \tag{3}$$

that becomes:

$$\epsilon_S = \frac{B+S}{S}\left(\epsilon_{S+B} - \frac{B}{S+B}\epsilon_B\right) \tag{4}$$

solving for ϵ_S.

The study of the composition of the *probe* muon candidates in the background sample shows that the background composition is identical under the peak and in the sidebands. This allows us to use the sidebands to estimate the muonID performance on the background under the peak.

Therefore, in order to estimate ϵ_B we use background events in $50 < |M_{\mu\mu} - M_{J/\psi}| < 300\,\mathrm{MeV}/c^2$ mass region. We find $\epsilon_B = (35.2 \pm 1.1)\%$. This rather high value is due to the fact that the background is mostly dominated by kaons and pions decays in flight. Putting all these numbers in Equation 4 we find $\epsilon_S = (96.0 \pm 1.4)\%$, which is compatible with expectation, thus validating our method for background subtraction.

The quoted statistical accuracy on ϵ_S, slightly above 1%, can be achieved by using ~ 3000 events selected in a $\pm 300\,\mathrm{MeV}/c^2$ mass window ($\sim 450\ J/\psi \to \mu\mu$ decays in $\pm 1\sigma$), which can be acquired in ~ 10 minutes in the low luminosity scenario (Table 6). By restricting the accepted mass window to $\pm 200\,\mathrm{MeV}/c^2$ we expect almost the same error, if we assume the same efficiencies for (S+B) and B and the same S/B ratio. A $\sim 10\%$ increase in the error is expected by downscaling by a factor ten the sidebands region.

On the other hand, a larger acceptance on the sidebands is preferable in the starting phase of the data taking, to better tune the selection on real data.

The same method used above to determine the average muonID efficiency can be used to determine the efficiency as a function of the probe track momentum by dividing the sample in momentum bins. The result is shown in Figure 10; with the present limited statistics (~ 10 minutes of data taking at low luminosity) we have chosen a rather coarse binning in order to limit the error per bin at few per cent.
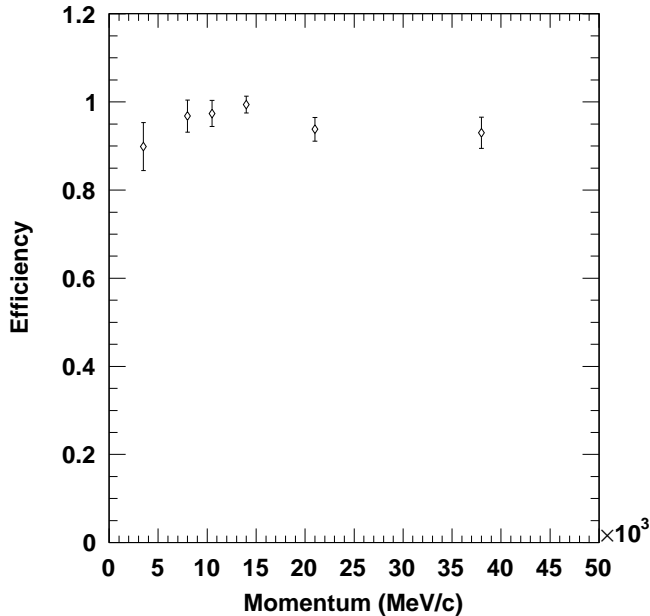
Figure 10: MuonID efficiency as a function of probe track momentum.

It could be envisaged, mainly at the start-up, to have a measurement of the muonID efficiency for each muon detector region and possibly, for each quadrant of each region in order to spot possible sources of inefficiency.

In Table 7 we show in the first two columns the percentage of probe muons impinging in each detector region and the sharing among the muon detector regions of the total ~ 5 Hz $J/\psi \to \mu\mu$ rate in ± 300 MeV/c^2 mass window in the low luminosity regime (Table 6). In the third column we show the time required to collect the 3000 J/ψ events necessary to perform an efficiency measurement at 1% level in each region.

Region	Illumination	Rate per region	Time per region
1	$\sim 6\%$	~ 0.3 Hz	2.8 h
2	$\sim 28\%$	~ 1.4 Hz	0.6 h
3	$\sim 36\%$	~ 1.8 Hz	0.5 h
4	$\sim 30\%$	~ 1.5 Hz	0.6 h

Table 7: Fraction of *probe* muons crossing a given muon detector region, rates and time necessary perform a measurement at 1% level per region.

5.5.1 MuonID efficiency measurement: systematic studies

The accuracy in the extraction of ϵ_S by using Equation 4 rests essentially on the reliability of the determination of S and B in the signal region, and of ϵ_B in the background sidebands.

This can be checked by using MC truth information.

In a $\pm 1\sigma$ mass window we obtain from fit S/B~ 5, with MC truth giving S/B~ 4.7. From this shift we expect from Equation 4 a systematic underestimation of ϵ_S of $\sim -1\%$, which gives most of the difference between ϵ_S and ϵ_S^{true} obtained above.

If we use instead a $\pm 2\sigma$ mass window to measure the efficiency and to count S and B, we get $\epsilon_S = (94.7 \pm 1.4)\%$ and $S/B \sim 3.5$, compared to true values of $(97.9 \pm 0.6)\%$ and ~ 3, respectively; again, the observed bias on S/B explains almost completely the underestimation of ϵ_S.

We also performed a similar test at much higher statistics on a sample of MC with artificial mixing of J/$\psi \to \mu\mu$ decays and MB events. Fitting the invariant mass spectrum, taking into account the radiative tail, we obtain in a $\pm 2\sigma$ mass window a value of S/B~ 9 compared to a true value of ~ 9.6, which leads to an overestimation of ϵ_S of $\sim 0.6\%$.

When ϵ_B is considered, the value obtained on the sidebands, $\epsilon_B = (35.2 \pm 1.1)\%$, is compared with the MC truth, $\epsilon_B^{true} = (34 \pm 1)\%$. This shift produces an underestimation of ϵ_S of $\sim 0.2\%$.

From this very preliminary investigation, we can conclude that a systematic accuracy at the level of few per mill on ϵ_S can be achieved, with a careful treatment of the mass invariant fit. In particular, when higher statistics become available, a better S/B ratio could also be tried, with a corresponding decrease in the systematic error. Moreover, analysis of higher statistical samples is needed to make more quantitative statements on this subject.

6 The $\Lambda(1115.6) \to p\pi^-$ calibration sample

The $\Lambda(1115.6) \to p\pi^-$ is a quite abundant process at LHC: at 14 TeV center-of-mass energy the prompt $pp \to \Lambda X, \overline{\Lambda} X$ processes have cross sections of $\sigma_{pp\to\Lambda X} \sim 10$ mb [11]. Given the branching ratio of $\Lambda, \overline{\Lambda} \to p\pi$, $BR(\Lambda \to p\pi) = (63.9 \pm 0.5)\%$ [8], we have a $\Lambda, \overline{\Lambda}(1115.6) \to p\pi$ decay every ~ 10 minimum bias events.

Since this process is very abundant it does not need a special trigger to be selected as it belongs to the underlying events of any triggered sample.

This decay is particularly interesting for studying the misID due to both decays and non-decays in flight, as it contains both a proton and a pion.

Moreover the Λ is a very narrow resonance ($\sigma(M) \sim 1$ MeV) and has a very long lifetime ($c\tau \sim 7.89$ cm) so it can be easily selected without any particle ID by using only tight cuts in impact parameters, flight distance and invariant mass.

6.1 The $\Lambda(1115.6) \to p\pi^-$ selection

The $\Lambda \to p\pi$ sample has been selected from a sample of 5.4×10^6 MB events after the L0 trigger.

The selection uses only kinematic variables and does not rely on any particle identification (PID) information. These variables are: the maximum and the minimum transverse momentum among the two daughter tracks ($p_{T,max}$), the minimum impact parameter χ^2 ($IP\chi^2_{min}$), the distance of the Λ decay vertex and primary vertex along the z axis, $dz = (z(\Lambda) - z(PV))$, and the cosine of the pointing angle[5] ($\cos(\theta)$). The distributions of $IP\chi^2_{min}$, dz and $\cos(\theta)$ are shown in Figure 11 separately for Λ decaying inside the VELO volume (LL category) and outside the VELO volume (DD category).

The $\Lambda(1115.6) \to p\pi^- (\overline{\Lambda}(1115.6) \to \overline{p}\pi^+)$ events have been selected from the minimum bias sample by requiring two tracks (LL or DD) of opposite sign, pointing inside the Muon detector acceptance and applying the cuts listed in Table 8.

As the biggest contribution to background events comes from $K_S \to \pi^+\pi^+$ events, a K_S veto is applied by rejecting all the track pairs with an invariant mass $|M_{\pi\pi} - M_{K_S}| < 30$ MeV/c^2 in the $\pi\pi$ hypothesis (Figure 12).

In Figure 13 we show the $M_{p\pi}$ invariant mass spectra for the LL and DD categories for events surviving the selection out of $\sim 5.4 \times 10^6$ DC06 minimum bias L0-yes. Results of a fit with double Gaussian shape for the signal (mean value μ, widths σ and σ_2, weights k_1 and k_3) and linear approximation for the background (intercept k_2 and slope α) are superimposed to the mass spectra. The number of candidates after the selection in a ± 20 MeV/c^2 mass window is shown in Table 9 separately for the LL and DD categories. Such a large mass window is necessary to evaluate the background in the sidebands and

---

[5]The pointing angle θ is the angle between the Λ momentum and the line of flight defined by the primary and decay vertexes.

cut	LL category	DD category
Decay products:		
$\chi^2_{\text{trk}}/\text{nDoF}$	< 2	< 2
$p_{\min}$	$> 3\,\text{GeV}/c$	$> 3\,\text{GeV}/c$
$p_{\text{T,min}}$	$> 100\,\text{MeV}/c$	$> 100\,\text{MeV}/c$
$p_{\text{T,max}}$	$> 200\,\text{MeV}/c$	$> 400\,\text{MeV}/c$
$IP\chi^2_{\min}$	> 5	> 5
Mother:		
dz = z(Λ) - z(PV)	50 mm<dz<600 mm	500 mm<dz<2200 mm
θ pointing	< 1 mrad	< 1.4 mrad
$\Delta M = |M_{\pi p} - M_\Lambda|$	$\Delta M < 20\,\text{MeV}/c^2$	$\Delta M < 20\,\text{MeV}/c^2$
K_S veto:	$|M_{\pi\pi} - M_{K_S}| > 30\,\text{MeV}/c^2$	$|M_{\pi\pi} - M_{K_S}| > 30\,\text{MeV}/c^2$

Table 8: $\Lambda(1115.6) \to \text{p}\pi^-$ selection cuts for the LL and the DD category.

interpolate it under the peak. The number of events used in the calibration is instead evaluated in a narrow mass window ($\pm 2\,\text{MeV}/c^2$) where the S/B ratio is ~ 33 and ~ 45 for the LL and DD categories, respectively (Table 9).

	LL category	DD category
N_{tot} (N_S) in ($\pm$ 20 MeV/c^2)	23800 (18000)	25600 (22400)
N_{tot} (N_S) in ($\pm$ 2 MeV/c^2)	18600 (16500)	18900 (18200)
S/B ($\pm$ 2 MeV/c^2)	~ 33	~ 45

Table 9: Number of $\Lambda(1115.6) \to \text{p}\pi^-$ candidates (signal events) selected from a sample of $\sim 5.4 \times 10^6$ MB events in a large (± 20 MeV/c^2) and the tight ($\pm$ 2 MeV/c^2) mass window. The S/B ratio is evaluated in $\pm$ 2 MeV/c^2. The two LL and DD categories are shown separately.

The momentum spectrum and the illumination of M2 station of the Λ decay products are shown in Figure 14 and Figure 15. In Table 10 we show in which fraction the Λ decay products cross a muon detector region.

Region 1	$\sim 7\,\%$
Region 2	$\sim 31\%$
Region 3	$\sim 37\%$
Region 4	$\sim 25\%$

Table 10: Fraction of Λ decay products crossing a given muon detector region.
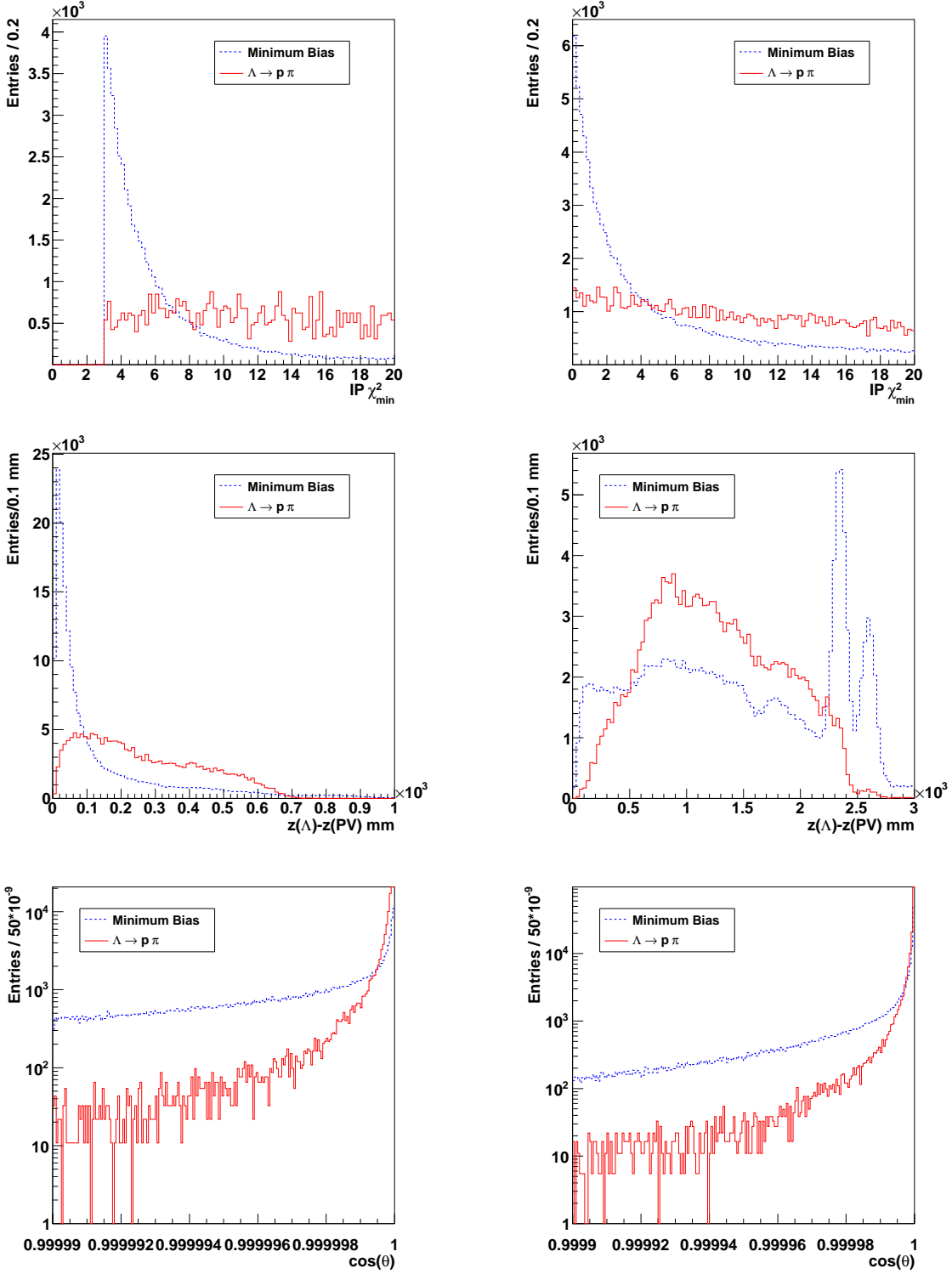
Figure 11: Distributions of the main variables (from top row $IP\chi^2_{\min}$, dz and $\cos(\theta)$) used in the $\Lambda(1115.6) \to p\pi^-$ selection for the LL category (left) and DD category (right), for signal (solid red line) and background (dashed blue line) events.
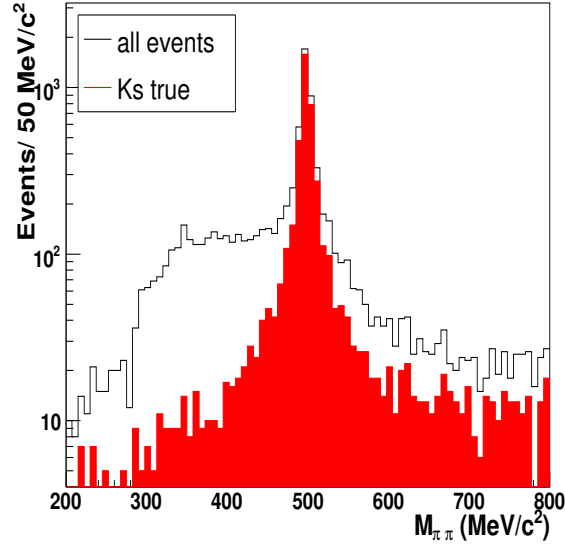
Figure 12: Invariant mass in the $\pi^+\pi^-$ hypothesis (solid line) for $\Lambda(1115.6) \rightarrow p\pi^-$ candidates extracted from a sample of minimum bias events. True Monte Carlo $K_S \rightarrow \pi\pi$ events are shown in the solid histogram.
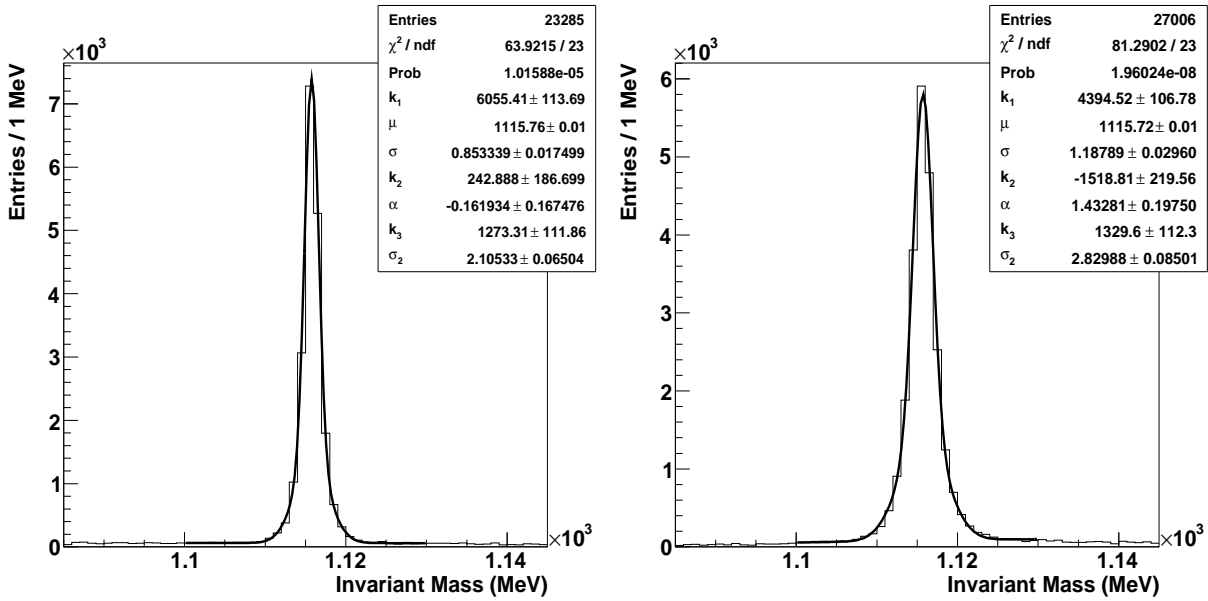

Figure 13: $M_{p\pi}$ invariant mass for LL-category (left) and DD-category (right) extracted from 5.4×10^6 MB events after L0-trigger. The meaning of the parameters of the fit is explained in the text.
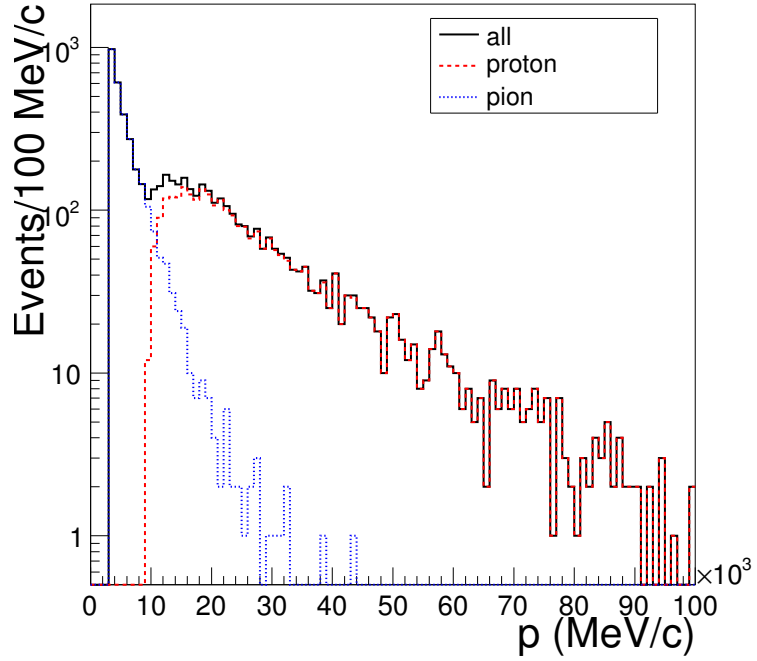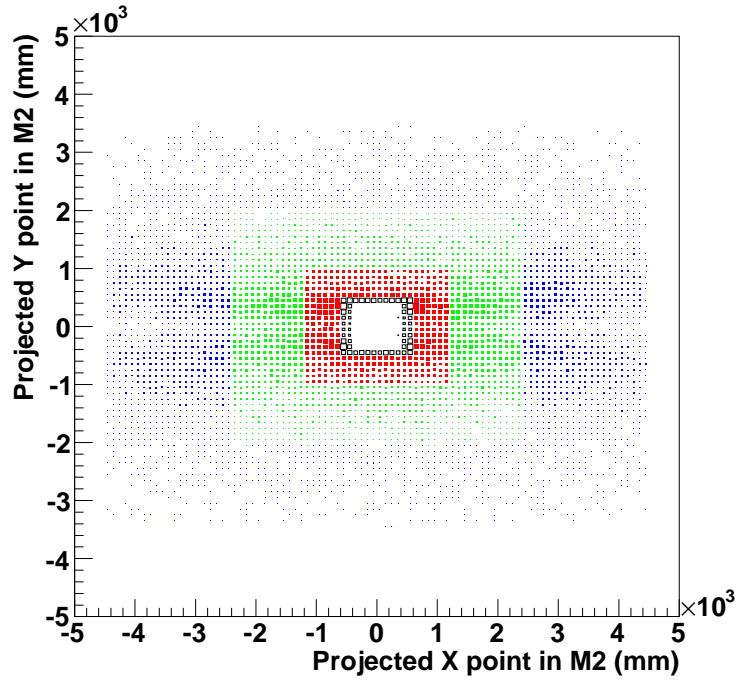
Figure 14: Momentum spectrum of the Λ decay products.

Figure 15: Muon detector illumination for the Λ decay products.

24

6.2 The proton-pion separation

The identification of the proton (anti-proton) and π^- (π^+) in the Λ ($\overline{\Lambda}$) decay can be performed by using only kinematic quantities.

In fact the large difference between the p and π masses results in a longitudinal momentum asymmetry $\Delta P = (p_L^+ - p_L^-)/(p_L^+ + p_L^-)$, where $p_L^\pm$ is the longitudinal momentum of the positive/negative track with respect to the Λ flight direction.

This is shown in Figure 16 where we plot the transverse momentum p_T of the decay products with respect to the Λ flight direction versus the ΔP variable for $\Lambda(1115.6) \rightarrow$ pπ^-, $\overline{\Lambda}(1115.6) \rightarrow \overline{p}\pi^+$ and $K_S \rightarrow \pi^+\pi^-$ decays [12].

Since the K_S decay is fully symmetric with respect to the exchange of positive and negative charged tracks, the ΔP distribution is centered to zero. On the contrary, the $\Lambda \rightarrow p\pi$ decays are not symmetric being $\Delta P < 0$ for $\overline{\Lambda}(1115.6) \rightarrow \overline{p}\pi^+$ and $\Delta P > 0$ for $\Lambda(1115.6) \rightarrow p\pi^-$.

The longitudinal momentum asymmetry variable provides a clever way to disentangle protons (anti-protons) from pions: in fact if the $\Lambda \rightarrow p\pi$ candidate has $\Delta P > 0$ the track of positive (negative) charge is the proton (pion). Vice-versa if $\Delta P < 0$.

The identification of protons and pions allows to separate the contribution of decays in flight from spurious hits or punch-through in the total misidentification rate.
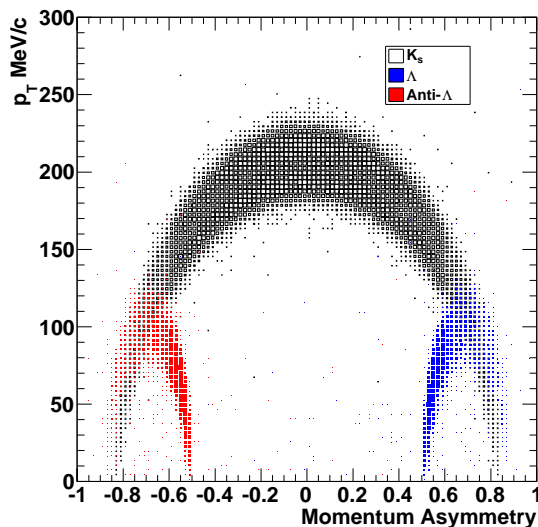

Figure 16: The Armenteros-Podolansky plot. The symmetric dark (blue) curve shows the Ks decays, the light (red) curve with $\Delta P < 0$ shows the $\overline{\Lambda}(1115.6) \rightarrow \overline{p}\pi^+$ decays and the light (red) curve with $\Delta P > 0$ shows the $\Lambda(1115.6) \rightarrow p\pi^-$ decays.

6.3 The $\Lambda(1115.6) \to p\pi^-$ rate

The number of candidates in a given mass window (Table 9) can be translated in a rate of events by following the same procedure used for the $J/\psi \to \mu\mu$ (Section 5.3).

In Table 11 we show, as for the $J/\psi \to \mu\mu$ control channel, the rate evaluated for the three running conditions expected for the 2009-2010 run and for nominal running conditions. The rates are calculated in the large mass window (± 20 MeV/c^2) in order to have enough sidebands for evaluating the background under the peak. Also in this case we assume a $\sqrt{s} = 14$ TeV center-of-mass energy and a L0-trigger with nominal settings.

At the nominal run conditions we have a total rate of ~ 4 kHz for both the LL and DD categories. For the other running scenarios we range from ~ 30 Hz in the lowest luminosity regime to ~ 600 Hz in the High luminosity regime. In all cases almost $\sim 80\%$ of the rate is pure signal. Different pre-scaling factors depending on the luminosity will be applied in order to fit to the allowed bandwidth dedicated to this channel of $\sim 5 - 10$ Hz.

	Low	Medium	High	nominal
L ($\times 10^{31}$ cm^{-2} s^{-1})	0.228	0.814	2.802	20
Bunches @ LHCb	19	68	468	2622
R_{BC} [kHz]	135.1	483.4	2070.8	14760
LL category				
total (signal) rate in ± 20 MeV/c^2 [Hz]	36 (27)	130 (100)	550 (420)	3900 (3000)
DD category				
total (signal) rate in ± 20 MeV/c^2 [Hz]	40 (34)	140 (120)	590 (520)	4200 (3700)

Table 11: Upper part: average luminosity, number of bunches colliding at LHCb and rates of minimum bias crossings corresponding to the running conditions expected in the 2009-2010 run (first three columns) and to the nominal running conditions (fourth column). Bottom part: total (signal) rate of $\Lambda(1115.6) \to p\pi^-$ ($\overline{\Lambda}(1115.6) \to \bar{p}\pi^+$) candidates after selection in ± 20 MeV/c^2 mass window.

6.4 The muon misidentification efficiency measurement

The muon misidentification efficiency evaluation is performed by selecting $\Lambda(1115.6) \to p\pi^-$ ($\overline{\Lambda}(1115.6) \to \bar{p}\pi^+$) candidates with a mass within a window of $\pm 2\sigma$ around the nominal Λ mass and by requiring both the pion and the proton candidates to pass the *IsMuonLoose* condition (Section 2).

We find a misidentification efficiency $\epsilon_{S+B} = (5.2 \pm 0.2)\%$ which is fully compatible with the result obtained when the events are selected using the Monte Carlo truth, $\epsilon_B = (4.8 \pm 0.2)\%$, due to the fact that the S/B ratio under the peak is very high.

26

The agreement is confirmed in each momentum bin, as can be seen in Figure 17 where we plot the misID efficiency as a function of the momentum for events selected with/without the Monte Carlo truth.

Then we can separate protons from pions by using the momentum asymmetry described in Section 6.2. The results are shown in Figure 18 (right): the selected pions are shown with blue open squares, the selected protons with red open diamonds. In the same Figure 18 (left) we show the momentum spectrum of proton and pions from selected Λ decays. We see that the pions affect for the misidentification rate at low momenta where the contribution of the decays in flight is dominant, while protons contribute to the misidentification rate at high momenta where the contribution of the decays in flight is negligible. The protons are a unique source of probes to quantify the contribution to the misID due to spurious hits in the muon chambers or punch-through particles.
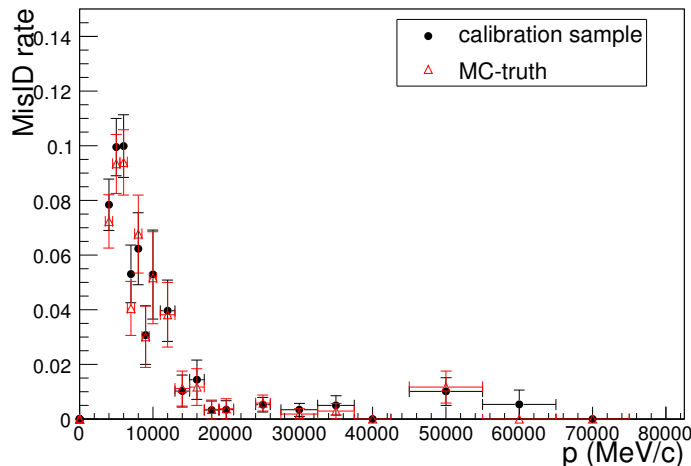

Figure 17: Muon misidentification efficiency after IsMuonLoose selector versus momentum for selected $\Lambda(1115.6) \rightarrow p\pi^-$ events: black dots are the results obtained from the calibration sample, red triangles are true signal events selected using Monte Carlo truth.
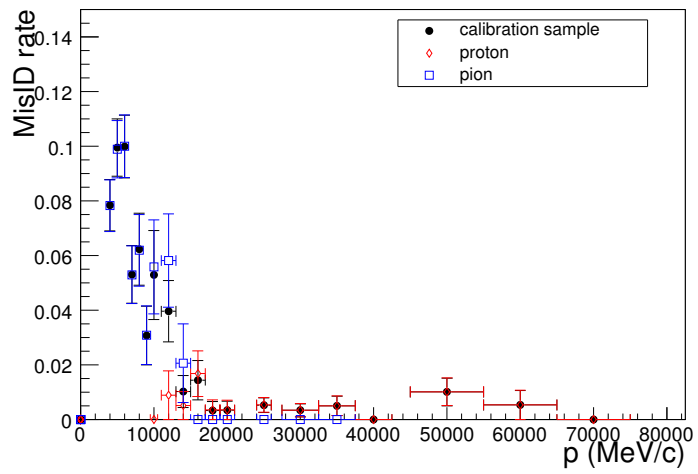
Figure 18: *IsMuonLoose* efficiency for $\Lambda(1115.6) \to p\pi^-$ events selected as explained in the text: blue squares show the efficiency for pions, red dots the efficiency for protons.

7 The calibration of the Fields of Interest

The calibration of the Fields of Interest requires the calibration of 40 curves, 3 parameters each for a total of 120 parameters [1].

These curves depend on the tracking parameters which define the track extrapolation into the muon system and on the multiple scattering, which depends on the momentum and the material crossed by the track.

For the FOI calibrations, at least 80k $J/\psi \rightarrow \mu\mu$ and 80k of $\Lambda(1115.6) \rightarrow p\pi^-$ events for each region are required [3]. In Table 12 we show the for the $J/\psi \rightarrow \mu\mu$ sample the percentage of probe muons impinging in each detector region and the sharing among the regions of a total ~ 4 Hz $J/\psi \rightarrow \mu\mu$ rate (medium luminosity scenario). In the third column we show the time required to collect the 80k J/ψ events per region necessary to perform a full calibration of the FOI parameters.

In Table 13 we show the same for the Λ events. In this case we assume a rate of ~ 5 Hz of Λ events which corresponds to an effective rate of ~ 10 Hz as both decay products can be used. However, the illumination of the protons and pions is quite asymmetric, being the protons (pions) mostly concentrated in the innermost (outermost) regions (Table 14).

The time required to collect the statistics necessary to perform a full FOI calibration is almost 1 day for R2-R3-R4 and 3.5 days for R1 for 5 Hz of $J/\psi \rightarrow \mu\mu$ and 5 Hz of $\Lambda(1115.6) \rightarrow p\pi^-$.

Therefore we plan to perform the full FOI calibration once at the beginning of data taking in order to spot possible differences between the detector description in the Monte Carlo and the data and then continuously monitor the muonID efficiency and misID rate.

If the performance is not stable, the FOIs will be enlarged/squeezed by a global factor in order to ensure the best possible working point for starting the reconstruction. In Figures 19- 20 we show how the muonID and misID curves change by applying different FOI factors.

The statistics required to monitor the muonID and misID efficiency at 5% relative accuracy is ~ 3000 $J/\psi \rightarrow \mu\mu$and ~ 3000 $\Lambda(1115.6) \rightarrow p\pi^-$, which corresponds to ~ 10 minutes of data taking at 5 Hz. A precise FOI parameters calibration aligned with the tracking parameters will be then performed offline.

Region	Illumination	Rate per region	Time per region
1	$\sim 6\%$	~ 0.24 Hz	~ 90 h
2	$\sim 28\%$	~ 1.1 Hz	~ 20 h
3	$\sim 36\%$	~ 1.4 Hz	~ 16 h
4	$\sim 30\%$	~ 1.2 Hz	~ 20 h

Table 12: $J/\psi \rightarrow \mu\mu$ sample: fraction of *probe* muons crossing a given muon detector region, rates and time needed to collect 80k probe muons per region. A total $J/\psi \rightarrow \mu\mu$ rate of 4 Hz is assumed.

Region	Illumination	Rate per region	Time per region
1	$\sim 17\%$	~ 1.7 Hz	~ 13 h
2	$\sim 29\%$	~ 2.9 Hz	~ 8 h
3	$\sim 26\%$	~ 2.6 Hz	~ 8 h
4	$\sim 28\%$	~ 2.8 Hz	~ 10 h

Table 13: $\Lambda(1115.6) \rightarrow p\pi^-$ sample: fraction of pions and protons crossing a given muon detector region, rates and time needed to collect 80k tracks per region. A total rate of $\Lambda(1115.6) \rightarrow p\pi^-$ of 5 Hz is assumed which corresponds to 10 Hz of useful tracks.

Region	Illumination (p and π)	Illumination (p only)	Illumination (π only)
1	$\sim 17\%$	$\sim 16\%$	$\sim 1\%$
2	$\sim 29\%$	$\sim 24\%$	$\sim 5\%$
3	$\sim 26\%$	$\sim 9\%$	$\sim 17\%$
4	$\sim 28\%$	$\sim 1\%$	$\sim 27\%$

Table 14: $\Lambda(1115.6) \rightarrow p\pi^-$ sample: muon detector illumination for protons and pions together and separately for the two components.
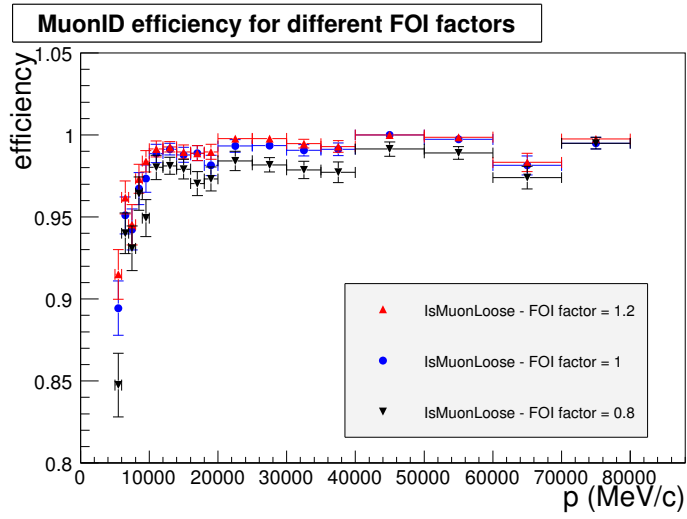
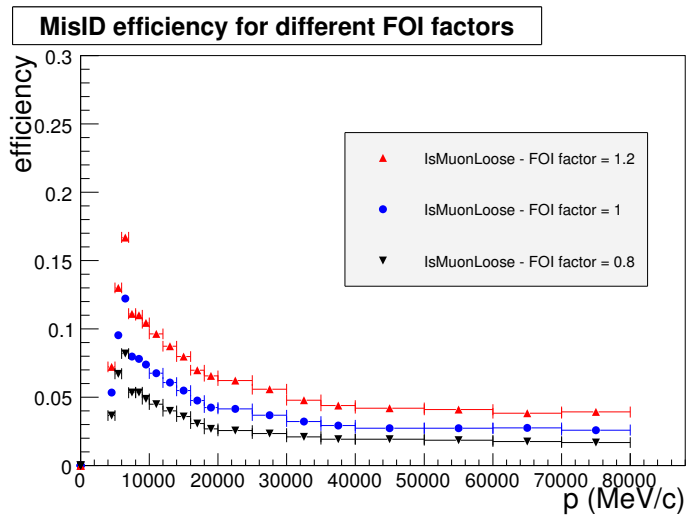Figure 19: Muon identification efficiency versus momentum for different FOI factors.

Figure 20: Muon misidentification efficiency versus momentum for different FOI factors.

8 The calibration of the DLL

The hypothesis test is performed by evaluating the probability for a given track of a given momentum p and impinging in a given muon detector region R to be a muon (P_μ or a non-muon ($P_{\text{non}-\mu}$) [1].

The P_μ and $P_{non-\mu}$ probabilities are then used to build up a Delta Log Likelihood variable defined as:

$$DLL = log\frac{P_\mu}{P_{non-\mu}}.$$

The main quantity used to build the P_μ ($P_{non-\mu}$) is the average squared distance of the hits in the muon chambers with respect to the track extrapolation:

$$D = \frac{1}{N} \sum_{i=0}^{N-1} \left\{ \left(\frac{x_{closest,i} - x_{track}}{pad_x} \right)^2 + \left(\frac{y_{closest,i} - y_{track}}{pad_y} \right)^2 \right\} \tag{5}$$

where the i runs over the fired stations of the *IsMuonLoose* definition and $x_{closest,i}, y_{closest,i}$ are the coordinates of the closest hit to the track extrapolation for that station.

The distribution of the D variable depends on the multiple scattering and, therefore, on the momentum of the track and the amount of crossed material by a given track, i.e. the polar angle. The dependence with p and polar angle (or muon detector region) is taken into account by binning the D distributions.

In Table 15 we show how the binning is defined for the J/$\psi \to \mu\mu$ sample: each muon detector region is divided into 4 or 5 momentum bins. The size and the number of the bins have been chosen as a compromise between the accuracy in the compensation of the momentum dependence and the time necessary to collect at least 2000 tracks per bin.

In Figure 21 we show the distributions of the average distance for two bins per region. The distributions obtained with a generic b-inclusive sample are compared with the ones obtained with the J/$\psi \to \mu\mu$ calibration sample.

In Table 16 we show the relative amount of J/$\psi \to \mu\mu$ selected events for each bin given by the convolution of the illumination of a given region and the momentum spectrum. For example, if we have a total rate of J/$\psi \to \mu\mu$ of $\sim$4 Hz, in the bin 2 of region 2 we have a rate of $4 \times 0.07 = 0.28$ Hz. Therefore the time required to accumulate at least 2000 tracks in this bin is $\sim$ 2 hours. This is the typical time necessary to calibrate the distance distributions for muons in regions R2, R3 and R4. For R1 we need ten times more time to accumulate the same statistics in each bin, i.e. $\sim$ 20 hours, as the illumination is ten times lower.

For hadrons, where the D dependence with p is weaker, we just divide in regions. The calibration of the D distance is done by using only the protons from the Λ decay in order to avoid the contamination of the π's decays in flight which have a D distribution very similar to the muons one. The protons have to pass the IsMuonLoose filter in order to be used for the DLL calibration. The efficiency of the filter for protons in Λ decays is typically

$\sim 1\%$. Therefore assuming ~ 5 Hz of $\Lambda(1115.6) \to \mathrm{p}\pi^-$ events we have $5 \times 0.01 = 0.05$ Hz of useful tracks. Given the illumination of protons shown in Table 14 we need 23, 35 and 55 hours to calibrate the distance distributions respectively in R1, R2 and R3-R4 together.

In conclusion, a complete calibration of the distance distributions for muons and non-muons can be provided every $\sim$ 2-3 days if the rate of $\mathrm{J}/\psi \to \mu\mu$ and $\Lambda(1115.6) \to \mathrm{p}\pi^-$ events is $\sim 4 - 5$ Hz, the bottleneck being the rate of protons after the IsMuonLoose selector in the outermost muon detector regions.

In Figures 22-23 we show the distributions for the P_μ, $P_{\mathrm{non}-\mu}$ and $DLL = log(P_\mu/P_{\mathrm{non}-\mu}$ obtained with muons and non-muons from a generic b-inclusive sample and from the $\mathrm{J}/\psi \to \mu\mu$ and $\Lambda(1115.6) \to \mathrm{p}\pi^-$ calibration samples: the distributions overlap nicely showing that the p, p_T dependence has been properly taken into account.

Region	bin 1 p [GeV/c]	bin 2 p[GeV/c]	bin 3 p [GeV/c]	bin 4 p [GeV/c]	bin 5 p [GeV/c]
R1	$3 - 30$	$30 - 40$	$40 - 50$	> 50	$-$
R2	$3 - 20$	$20 - 30$	$30 - 40$	$p > 40$	$-$
R3	$3 - 10$	$10 - 20$	$20 - 30$	$p > 30$	$-$
R4	$3 - 6$	$6 - 8$	$8 - 10$	$10 - 15$	$p > 15$

Table 15: Definitions of momentum bins for the $\mathrm{J}/\psi \to \mu\mu$ sample.

Region	bin 1 [%]	bin 2 [%]	bin 3 [%]	bin 4 [%]	bin 5 [%]
R1	0.8	0.7	0.7	1.2	$-$
R2	6	7	6	7	$-$
R3	7	17	8	4	$-$
R4	6	7	6	8	4

Table 16: Relative amount of probe muons from $\mathrm{J}/\psi \to \mu\mu$ events in each bin.
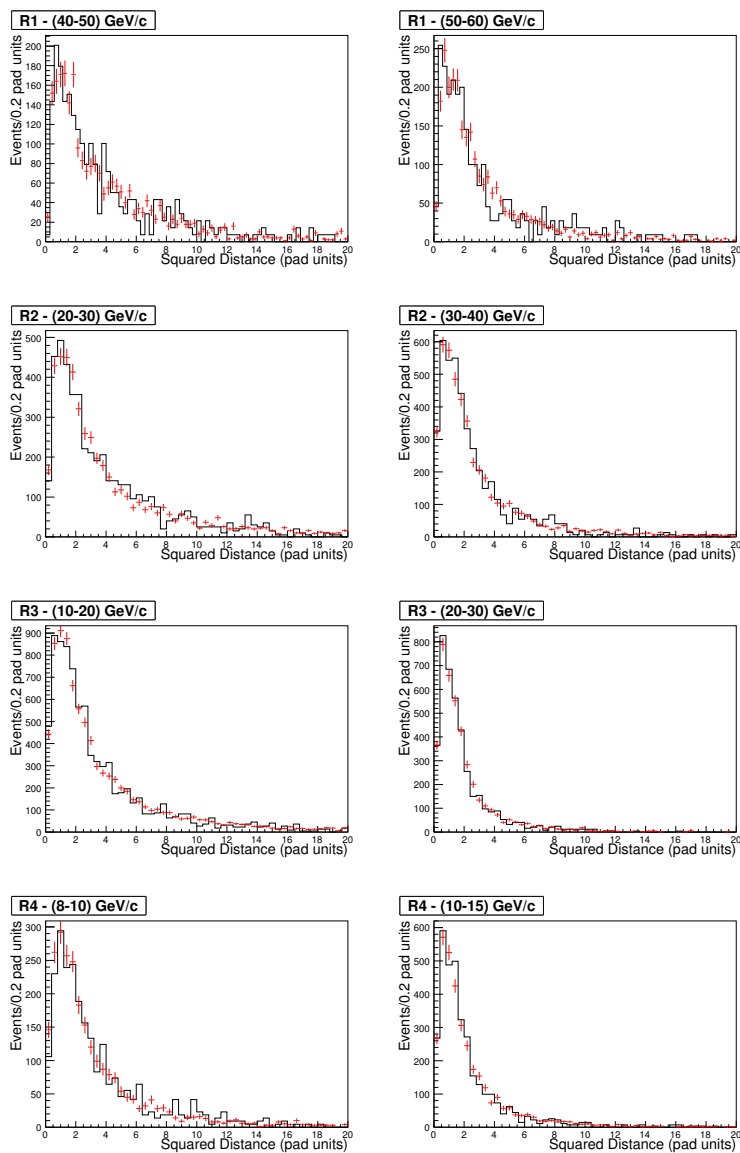
Figure 21: Average distance distributions for two bins per region. The distributions obtained with a generic *b*-inclusive sample (solid histogram) are compared with the ones obtained with the J/$\psi \rightarrow \mu\mu$ calibration sample (filled circles).
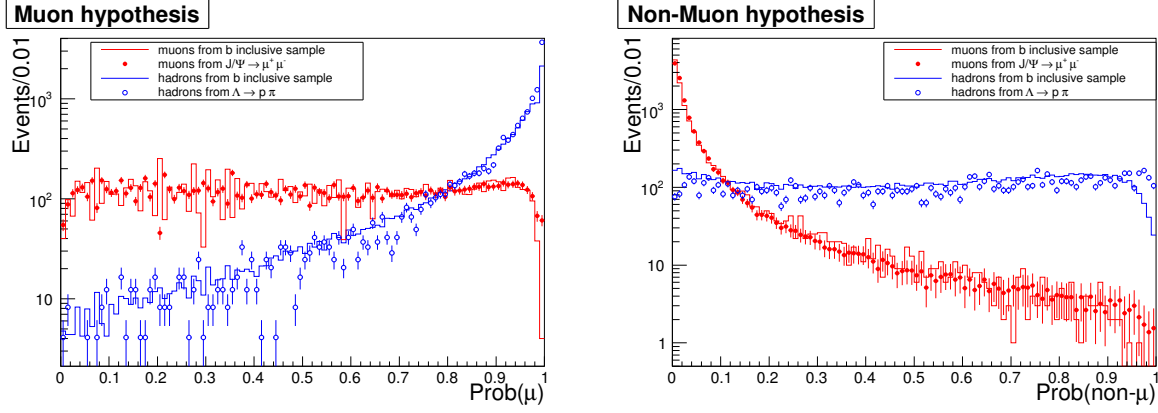
Figure 22: Left: Probability to be a muon for muons and hadrons (non-decaying in flight) samples. Right: Probability to be a non-muon for muons and hadrons (non-decaying in flight) samples. Solid histograms are from a generic b−inclusive sample, dots from $J/\psi \to \mu\mu$ and $\Lambda(1115.6) \to p\pi^-$ calibration samples.
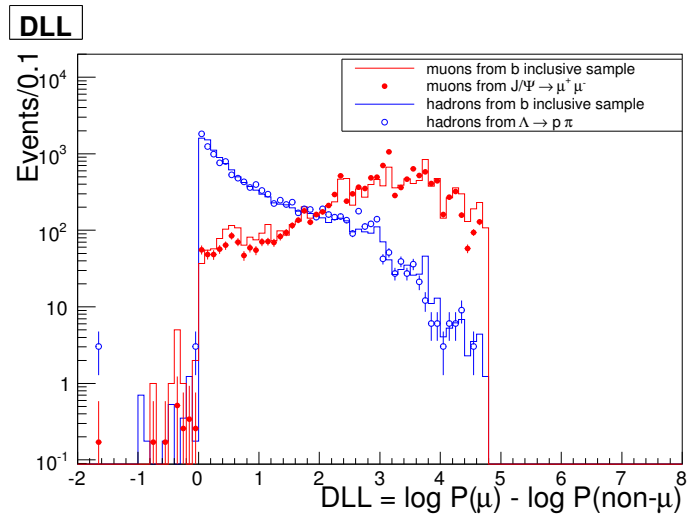

Figure 23: Delta Log Likelihood for muons and non-muons samples. Solid histograms are from a generic b−inclusive sample, dots from $J/\psi \to \mu\mu$ and $\Lambda(1115.6) \to p\pi^-$ calibration samples.

9   Conclusions

We presented a strategy for calibrating with data the LHCb muon identification procedure and for extracting in-situ the performance.

In the first period of data taking we plan to use two main calibration samples: the inclusive $J/\psi \to \mu\mu$ decay as a source of muons and the $\Lambda(1115.6) \to p\pi^-$ decay as a source of hadrons decaying and non-decaying in flight.

For each of them we have described the trigger lines, the offline selection, the expected purity and the rates for different running scenarios. The statistics collected is a function of the trigger and offline bandwidths dedicated to these two channels: we have assumed conservatively ~ 5 Hz of $J/\psi \to \mu\mu$ and ~ 5 Hz of $\Lambda(1115.6) \to p\pi^-$.

With these rates the average muonID efficiency can be measured with a precision of $\sim 1\%$ and the average misID rate with a precision of few per mil with the statistics collected in few minutes of data taking.

The full calibration of the muonID procedure requires a data set corresponding to 2-3 days of data taking with the rates assumed above. Therefore the full calibration will be done once at the beginning and then periodically if the performance is not stable.

The muonID procedure takes properly into account the momentum dependence therefore all the relevant distributions can be extracted from the calibration samples and exported to any signal sample without corrections.

10   Acknowledgements

References

[1] G. Lanfranchi, X. Cid Vidal, S. Furcas, M. Gandelman, J. A. Hernando, J. H. Lopez, E. Polycarpo and A. Sarti
The Muon Identification Procedure for the LHCb experiment with the first data, LHCb-PUB-2009-013.

[2] A. Bates et al., *Road map for charmless charged two-body B decays at LHCb.*

[3] E. Polycarpo, M. Gandelman, *The Performance of the LHCb Muon Identification Procedure*, LHCb note 2007-145 (2007).

[4] The LHCb Collaboration, *The LHCb Technical Proposal*, CERN/LHCC 98-004.

[5] D. Acosta et al., *Measuring Muon Reconstruction efficiency from Data*, CMS NOTE 2006/060.

[6] The ATLAS Collaboration, *Expected Performance of the ATLAS experiment*, CERN-OPEN-2008-020.

[7] https://twiki.cern.ch/twiki/bin/view/LHCb/SettingsDC06.

[8] C. Amsler et al. (Particle Data Group), Phys. Lett. **B 667**, 1 (2008).

[9] *LHCb Calorimeters, Technical Design Report*, CERN-LHCC-2000-049.

[10] I. Korolko et al., *On the possibility of in-situ calibration of LHCb calorimeters*, CERN-LHCb-2000-051.

[11] M. Schmelling, plenary session at the LHCb week, January 2008
http://indico.cern.ch/conferenceDisplay.py?confId=26118

[12] J. Podolanski and R. Armenteros, Phil. Mag. **45** (1954), 13.